HAL
open science

# Dynamical influence of the Tibetan Plateau on the winter monsoon over southeastern Asia

Sylvain Mailler, François Lott

## To cite this version:

Sylvain Mailler, François Lott. Dynamical influence of the Tibetan Plateau on the winter monsoon over southeastern Asia. Geophysical Research Letters, 2009, 36, 10.1029/2008GL036952 . hal-04113777

**HAL Id: hal-04113777**

**https://hal.science/hal-04113777v1**

Submitted on 2 Jun 2023

**HAL** is a multi-disciplinary open access archive for the deposit and dissemination of scientific research documents, whether they are published or not. The documents may come from teaching and research institutions in France or abroad, or from public or private research centers.

L'archive ouverte pluridisciplinaire **HAL**, est destinée au dépôt et à la diffusion de documents scientifiques de niveau recherche, publiés ou non, émanant des établissements d'enseignement et de recherche français ou étrangers, des laboratoires publics ou privés.

Copyright

# Dynamical influence of the Tibetan Plateau on the winter monsoon over southeastern Asia

Sylvain Mailler[1,2] and François Lott[1]

Received 10 December 2008; accepted 24 February 2009; published 26 March 2009.

[1] Previous studies have shown (1) that the Tibetan Plateau produces a significant fraction of the two components of the Equatorial Mountain Torque (EMT) in winter, (2) that these torques are in part related to the East Asian cold surges, and (3) that the cold surges affect the convection over the maritime continent. We show here that these relations are strong enough for the convection over the Equatorial South China Sea to be associated with significant signals on the two components of the EMT that can precede by a few days and more the convection. These signals are associated to surface pressure and temperature patterns that are strongly reminiscent of the East Asian cold surges. Our results therefore show that the Tibetan Plateau couple dynamically the midlatitudes and the tropical region, and that the vectors of this dynamical coupling are the cold surges. This coupling also influences the convection over the northern Bay of Bengal, mainland southeast Asia, and Indonesia.
**Citation:** Mailler, S., and F. Lott (2009), Dynamical influence of the Tibetan Plateau on the winter monsoon over southeastern Asia, *Geophys. Res. Lett.*, *36*, L06708, doi:10.1029/2008GL036952.

## 1. Introduction

[2] During the northern winter, the weather in eastern Asia, the South China Sea (SCS) and the maritime continent is dominated by the winter monsoon, where the active monsoon phase is characterized by northerly low-level winds along the East Asian coasts extending from Japan to the SCS. This monsoon is also associated to intense convective events over the SCS and Borneo [*Houze et al.*, 1981; *Murakami*, 1980]. The variability of this monsoon has tropical and extratropical influences. It is modulated by the major modes of the equatorial variability, like the El Niño Southern Oscillation [see *Chang et al.*, 2004] and the Madden-Julian oscillation (MJO) [*Ichikawa and Yasunari*, 2006]. At shorter timescales, *Chang et al.* [2005] have shown that the Borneo vortex intensity and the cold surges can be as important as the MJO in modulating this monsoon. For the cold surges, this effect was also noticed by *Chang and Lau* [1980] and *Chang et al.* [1979], who have shown that the cold surges are followed by increased convection over the equatorial South China Sea (ESCS), while *Johnson and Priegnitz* [1986] have analyzed a particular case in Dec. 1978 of a cold surge influencing the cloud cover over the SCS. These observational results have also been reproduced in GCM simulations by *Slingo* [1998].

[1]Laboratoire de Météorologie Dynamique, IPSL, École Normale Supérieure, CNRS, Paris, France.
[2]École Nationale des Ponts et Chaussées, Marne la Vallée, France.

Copyright 2009 by the American Geophysical Union.
0094-8276/09/2008GL036952

[3] The cold surges are an important factor of the winter variability along the eastern slopes of at least three major mountain ranges: the complex formed by the Himalayas and the Tibetan Plateau (for conciseness, this complex will be named "Tibetan Plateau" in the following), the Andes and the Rockies [*Hsu and Wallace*, 1985; *Garreaud*, 2001]. In the case of the East Asian cold surges, they last 5 to 14 days, and a characteristic duration for the strong events is 9 days [*Zhang et al.*, 1997]. Statistical studies [e.g., *Murakami*, 1981] as well as numerical simulations [*Murakami and Nakamura*, 1983; *Nakamura and Murakami*, 1983; *Sumi*, 1983] have shown that the orographic effects are a crucial part of the East Asian cold surge dynamics. However, they did not consider the EMT signals associated to these transient phenomena, or their tropical implications.

[4] In mountain meteorology, it is quite common to measure the dynamical influence of mountains on the atmosphere by forces [*Davies and Phillips*, 1985]. In the midlatitudes and for large mountain ranges, a good fraction of these forces is due to the surface pressure patterns that are in geostrophic balance with the wind [*Smith*, 1979]. As this process can trigger baroclinic wave development and force planetary scale waves, these mountain forces need to be represented properly in the Numerical Weather Prediction models and the General Circulation Models [*Lott*, 1999].

[5] If we adopt a planetary scale approach, which is mandatory for massifs of the scale of the Tibetan Plateau, the Equatorial Atmospheric Angular Momentum budget [e.g., *Feldstein*, 2006] is a well closed framework to analyze these forces: if there is a positive surface pressure anomaly to the North of the Tibetan Plateau, it yields a positive torque ($T_{M,1}$) along the equatorial axis of the Earth that crosses the Greenwich meridian. A positive pressure anomaly to the East yields a negative torque ($T_{M,2}$) along the equatorial axis located at 90°E.

[6] For the Tibetan Plateau, *Egger and Hoinka* [2000, 2008] have shown that this mountain range produces substantial signals in $T_{M,1}$ and $T_{M,2}$ that are in lead-lag relationship (a signal in $T_{M,1}$ being followed by a signal in $T_{M,2}$ of the opposite sign). As the cold surges are associated with surface pressure anomalies that travel from the Northern flank of the Tibetan Plateau and intensify on the eastern flank, we will show that this relation between $T_{M,1}$ and $T_{M,2}$ is often related to the cold surges (this was only suggested by *Egger and Hoinka* [2008]).

[7] The object of this letter is to show that the dynamical forcing of the Tibetan Plateau on the East Asian winter monsoon is strong enough to have a direct impact on convection over a major monsoon variability center, the Equatorial South China Sea. To establish this, we will show that the convective events over the ESCS are often preceded by a few days by significant signals on $T_{M,1}$ and $T_{M,2}$; we will also show that

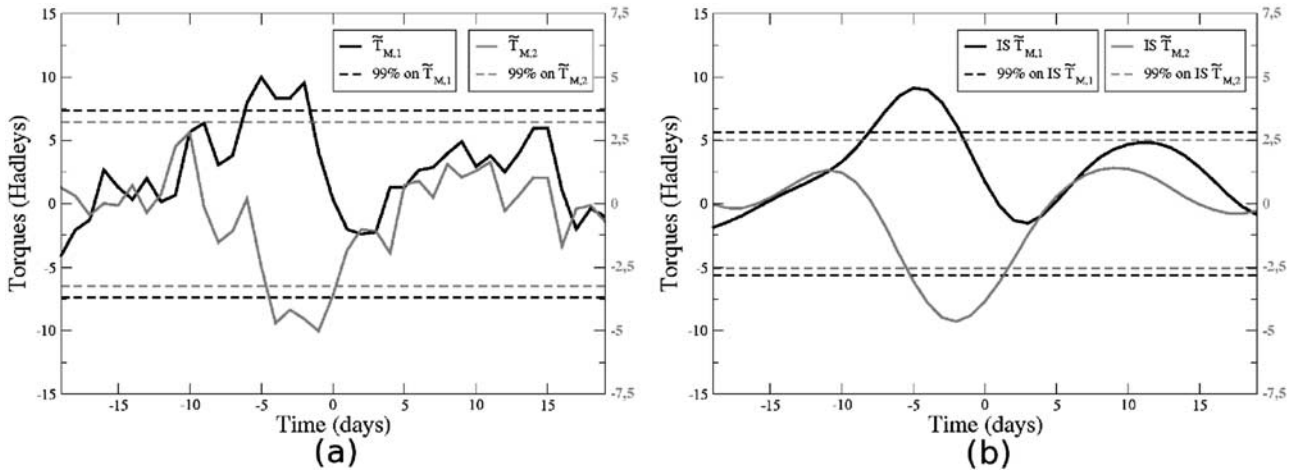


**Figure 1.** (a) Composite series of $\widetilde{T}_{M,1}$ (black solid) and $\widetilde{T}_{M,2}$ (gray solid) keyed on $\widetilde{I}_C$. Units for the torques are in Hadley: 1 H = $10^{18}$ kg m$^2$ s$^{-2}$. The dotted lines correspond to the 99% significance level for $\widetilde{T}_{M,1}$ (black) and $\widetilde{T}_{M,2}$ (gray). (b) Same as Figure 1a but for the IS $\widetilde{T}_{M,1}$ and $\widetilde{T}_{M,2}$. The convection events retained for Figure 1b are the same as for Figure 1a.

the vectors of this relationship between the Tibetan Plateau and the monsoon convection are the cold surges. Finally, we will show that the dynamical effect of the Tibetan Plateau's EMT on tropical convection is not limited to the ESCS, but also concerns the northern Bay of Bengal, mainland southeast Asia, and Indonesia.

## 2. Data and Methods

[8] To reveal that the convection over the ESCS is affected by the EMT generated by the Tibetan Plateau, we will use the daily data of the temperature at the .995 sigma level, $T_{50m}$, and of the surface pressure, $P_S$, both from the NCEP/NCAR reanalysis [*Kalnay et al.*, 1996]. To characterize the convection, we will use the daily data of the Outgoing Longwave Radiation from the NOAA interpolated OLR data set [*Liebmann and Smith*, 1996], hereinafter OLR in the text or $R_l$ in the Equations. From both data sets, we will analyze the 29 years over which they overlap (1979–2007).

[9] As we are interested in the dynamics of the intraseasonal and synoptic variations of convection, these two data sets will be filtered in two steps. First the annual cycle is removed and second a Lanczos high-pass filter [*Duchon*, 1979] is applied to remove the interannual variations. The half-power point of this filter is chosen at .005 *cycles/day*, which removes all the interannual variations but does not affect the IS and synoptic variations. The length of the filter weighting function is chosen at 601 days. In the following, the resulting filtered series will be called subseasonal and written $\widetilde{T}_{50m}$, $\widetilde{P}_S$ and $\widetilde{R}_l$. To build an index of the convective activity over the ESCS, we average the opposite of $\widetilde{R}_l$ over a sector ranging from 105°E to 120°E and from the equator to 15°N, which largely dubs the ESCS,

$$\widetilde{I}_C = -\frac{1}{S}\int_{0^\circ N}^{15^\circ N}\int_{105^\circ E}^{120^\circ E}\widetilde{R}_l a^2 \cos\phi \, \mathrm{d}\lambda \mathrm{d}\phi, \tag{1}$$

where $S$ is the surface of the sector, $\lambda$ is the longitude, $\phi$ the latitude, and $a$ is the Earth radius.

[10] With this definition, positive values of $\widetilde{I}_C$ correspond to a low OLR, and negative values of $\widetilde{I}_C$ correspond to a high OLR.

[11] The two components of the EMT due to the Tibetan plateau are computed following [*Feldstein*, 2006]:

$$\widetilde{T}_{M,1} = a^2 \int\int_{\phi,\lambda} \widetilde{P}_S(\lambda,\phi)\left(-\sin\lambda\frac{\partial Z_s}{\partial\phi} + \cos\lambda\tan\phi\frac{\partial Z_s}{\partial\lambda}\right) \cdot \cos\phi \, d\phi \, d\lambda, \tag{2}$$

$$\widetilde{T}_{M,2} = a^2 \int\int_{\phi,\lambda} \widetilde{P}_S(\lambda,\phi)\left(\cos\lambda\frac{\partial Z_s}{\partial\phi} + \sin\lambda\tan\phi\frac{\partial Z_s}{\partial\lambda}\right) \cdot \cos\phi \, d\phi \, d\lambda, \tag{3}$$

where $Z_s$ is the surface elevation. Note that the integrals in equations (2) and (3) are restricted to the sector [60°E; 120°E] × [15°N; 55°N] which includes all the Tibetan Plateau and the Himalayas.

[12] As the Tibetan Plateau is centered near the longitude 90°$E$, a positive $\widetilde{T}_{M,1}$ results from a positive South-North pressure gradient over the topography while a negative $\widetilde{T}_{M,2}$ is associated to a West-East positive pressure gradient. Note that positive West-East pressure gradients also produce a positive polar torque $\widetilde{T}_{M,3}$ [*Lott et al.*, 2004].

[13] The composite maps and series of Figures 1 and 2 are built using the 20 strongest positive peaks and the 20 strongest negative peaks of $\widetilde{I}_C$ from November through March (NDJFM) during the 1979–2007 period. According to *Zhang et al.* [1997], we only select dates from November to March (NDJFM), these months being the most suitable to study the East Asian winter monsoon and the cold surges. A minimum separation of 20 days between two successive peaks of $\widetilde{I}_C$ has been imposed to ensure that successive events are statistically independent. This allows to use a Student t-test to evaluate the confidence levels.

[14] The minimum OLR values associated to the positive peaks of $\widetilde{I}_C$ are very low (from 93 Wm$^{-2}$ to 130 Wm$^{-2}$) and correspond to brightness temperatures from 201 K to 219 K.



19448007, 2009, 6, Downloaded from https://agupubs.onlinelibrary.wiley.com/doi/10.1029/2008GL036952 by Cochrane France, Wiley Online Library on [02/06/2023]. See the Terms and Conditions (https://onlinelibrary.wiley.com/terms-and-conditions) on Wiley Online Library for rules of use; OA articles are governed by the applicable Creative Commons License

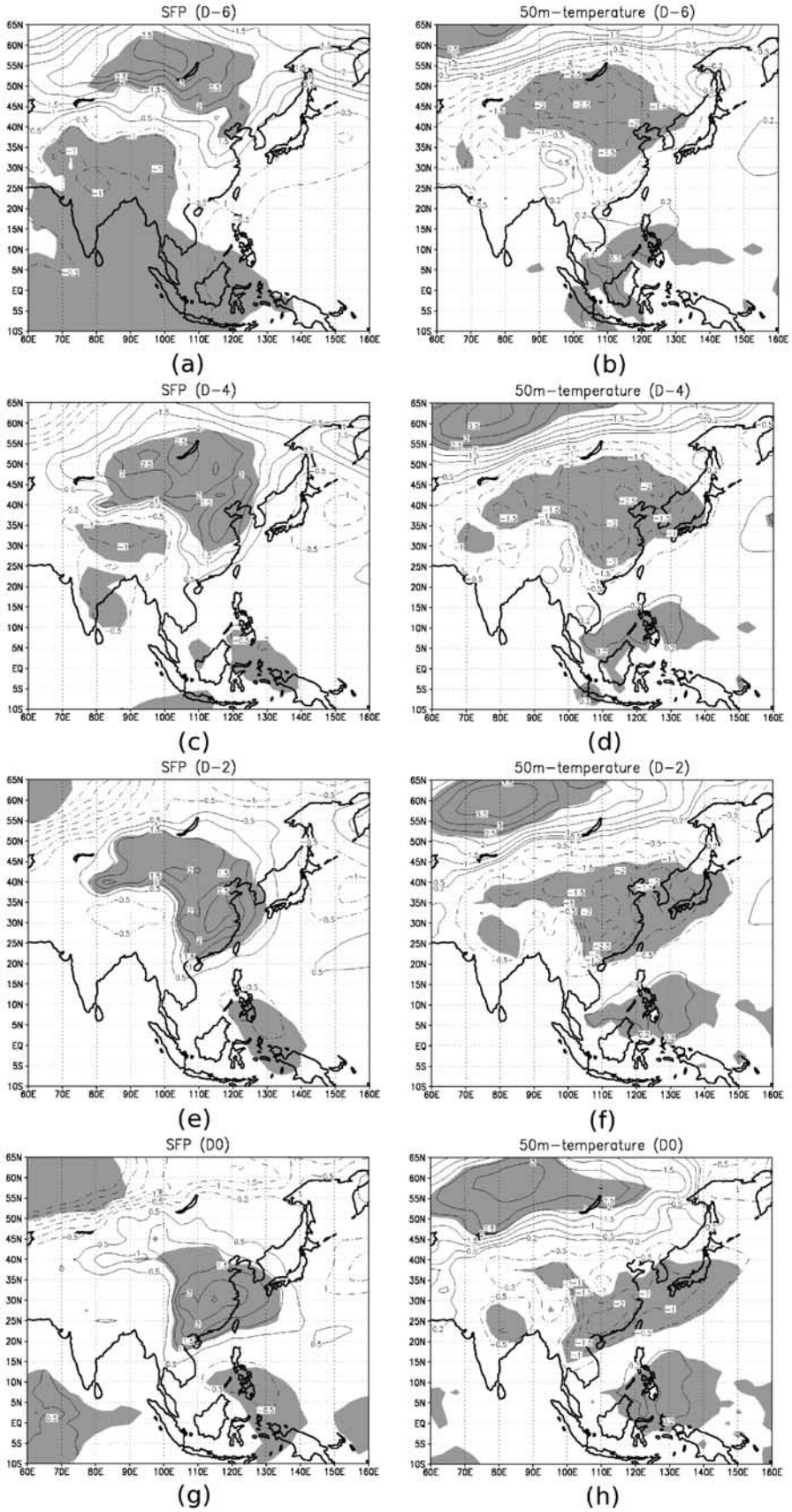


**Figure 2.** Composites of the IS $\widetilde{P}_S$ (hPa) and of the IS $\widetilde{T}_{50m}$ (K) keyed on $\widetilde{I}_C$. Contour interval: (left) 0.5 hPa and (right) 0.5 K; positive values, light solid; negative values, light dotted; 99% confidence, shaded; and continental contours, heavy solid. The days are counted from the local extremum of $\widetilde{I}_C$ (see text for details).



19448007, 2009, 6, Downloaded from https://agupubs.onlinelibrary.wiley.com/doi/10.1029/2008GL036952 by Cochrane France, Wiley Online Library on [02/06/2023]. See the Terms and Conditions (https://onlinelibrary.wiley.com/terms-and-conditions) on Wiley Online Library for rules of use; OA articles are governed by the applicable Creative Commons License

According to *Fu et al.* [1990], it is very likely that these low values are due to deep convection.

[15] The time lags are expressed in days relative to the peaks in $\widetilde{I}_C$: D0 is the day when $\widetilde{I}_C$ peaks and D-3 is three days before.

## 3. Equatorial Torques Due to the Tibetan Plateau

[16] The composites of the subseasonal series $\widetilde{T}_{M,1}$ and $\widetilde{T}_{M,2}$ keyed on the convection index, $\widetilde{I}_C$, are shown in Figure 1a. In it we can see that there is a significant positive anomaly in $\widetilde{T}_{M,1}$ from D-6 to D-2 which peaks at D-5. After this peak in $\widetilde{T}_{M,1}$, Figure 1a shows that $\widetilde{T}_{M,2}$ becomes negative, and this lasts from D-4 to D0.

[17] To characterize more precisely the timescales over which the convection over the ESCS and the torques are related, it is noticeable in Figure 1a that the peaks in $\widetilde{T}_{M,1}$ and $\widetilde{T}_{M,2}$ are significant during 5 days, and thereafter return to zero in around 5 days. These rather slow variations therefore have characteristic periods around 20 days (from peak to peak), which means that they can be extracted by the *Blackmon* [1976] low-pass filter that separates the high frequencies (periods below 10 days) from the low frequencies (periods above 10 days). Hereinafter, the resulting low-pass filtered series will be referred to as intraseasonal (IS). It is important to emphasize here that the IS series of $\widetilde{T}_{M,1}$, $\widetilde{T}_{M,2}$, and $\widetilde{I}_C$ capture around 60% of the variance of the unfiltered series $T_{M,1}$, $T_{M,2}$, and $I_C$ with annual cycle substracted. As expected, both IS $\widetilde{T}_{M,1}$ and IS $\widetilde{T}_{M,2}$ have strong signals a few days before the convective events (Figure 1b), with a significant positive signal on the Greenwich component ($\widetilde{T}_{M,1}$) peaking at D-5, followed by a negative signal on $\widetilde{T}_{M,2}$ peaking at D-2. This succession of a positive signal on the IS $\widetilde{T}_{M,1}$ and of a negative signal on the IS $\widetilde{T}_{M,2}$ is for us the evidence that the Tibetan Plateau often applies a strong dynamical forcing to the air masses during the week that precedes convection over the ESCS.

## 4. Composites of the Temperature and Surface Pressure Fields Before the Convective Events Over the ESCS

[18] The composite maps of the IS $\widetilde{P}_S$ and of the IS $\widetilde{T}_{50m}$ during the week before the convection peaks are in Figures 2 (left) and 2 (right), respectively. At D-6, a significant high pressure anomaly is forming with maximum value around 3.5 hPa in southern Siberia (Figure 2a). At the same time, a low temperature anomaly, with minimum value around 3 K, is extending from southern Siberia to the Korean Peninsula (Figure 2b). The following days (Figures 2c–2h), these anomalies in $\widetilde{P}_S$ and $\widetilde{T}_{50m}$ extend in size and gain in significance: at D-4, the high pressure anomaly is significant over southern Siberia, Mongolia and Northeastern China, which creates the peak of the IS $\widetilde{T}_{M,1}$ at that time (Figure 1b). At the same time, the temperature anomaly becomes significant over most of the eastern China (Figure 2d).

[19] At D-2, the high pressure has moved southeastward along the slopes of the Tibetan Plateau (Figure 2e), giving rise to the negative peak on $\widetilde{T}_{M,2}$ observed on Figure 1b. At the same time, the temperature is dropping over all eastern China, the East China Sea and southern Japan (Figure 2f). It is important to emphasize here that this pattern is typical of the East Asian cold surges [see *Zhang et al.*, 1997, Figure 7].

[20] The IS surface patterns associated with heavy wintertime convective events over the ESCS are in Figures 2g and 2h, respectively. The IS surface pressure at D0 (Figure 2g) is characterized by a large positive anomaly with maximal value around 2.5 hPa, centered at 30°N and covering the eastern China and down to the northern coast of the SCS. It almost coincides with a cold anomaly with maximal value around 2 K (Figure 2g). Again, it is important to note that this association of high pressure and low temperature anomalies over eastern China and the northern coast of the SCS is strongly reminiscent of the signals observed near the end of the life cycle of the cold surges [*Zhang et al.*, 1997]. This shows that there is a very significant link between convection in the ESCS and the occurrence of a cold surge 2 to 4 days before.

[21] During all this evolution, a low pressure anomaly seems to be moving eastward in the tropics, from the Indian ocean at D-6 and D-4 to the Philippines and the Western Pacific at D-2 and D0. This evolution may be related to the MJO, which is also known to influence convection over the ESCS in winter [*Ichikawa and Yasunari*, 2006]. This suggests that it is the combination of large scale tropical anomalies traveling eastward and of the anomalies coming from the midlatitudes and related to the Tibetan Plateau that results in intense convection over the ESCS.

## 5. Case Study and Influence Over Other Tropical Regions

### 5.1. A Strong Convective Event in November 1990

[22] To show the significance of our results for individual meteorological events, we next analyze a particular case. It corresponds to the week before 14 November 1990, a date for which the OLR is below 120 $Wm^{-2}$ over the north of the ESCS, which denotes the presence of deep convective tropical clouds according to *Fu et al.* [1990]. This event is also the third strongest peak of $\widetilde{I}_C$ in the period we study.

[23] The days before the convection peaks, we can see on Figure 3 that there is a strong signal on $\widetilde{T}_{M,1}$ from D-7 to D-5, followed by a strong signal on $\widetilde{T}_{M,2}$ from D-5 to D-3 (here strong means more than 3 times larger than the standard deviations in each series). To characterize that a cold surge also develops during this period, we follow *Zhang et al.* [1997] and average the surface temperature over the sector [112.5°E; 117.5°E] × [25°N; 30°N]. In Figure 3b we see that this quantity has decreased by 12 K, which is twice the 6 K threshold proposed by *Zhang et al.* [1997] to characterize cold surges. According to *Zhang et al.* [1997], there is also a threshold on sea level pressure over southern Siberia which is largely met in our case. This shows that, in this example, the evolutions of $\widetilde{T}_{M,1}$ and $\widetilde{T}_{M,2}$ are associated to a very strong cold surge, the latter occurring 4 days before the convection peaks. We can also note on Figure 3 that the signals in the EMT components and the averaged surface temperature last several days, in agreement with the time scales of the IS composites in Figure 1b.

### 5.2. Composites Keyed on the Himalayan Equatorial Torque

[24] In sections 3 and 4, we have analyzed the composites of the EMT components as well as of $\widetilde{P}_S$ and $\widetilde{T}_{50m}$ keyed on the OLR in the ESCS. To strengthen the results found in these sections, we now proceed the other way round and build composites of the OLR keyed on the EMT components.



19448007, 2009, 6, Downloaded from https://agupubs.onlinelibrary.wiley.com/doi/10.1029/2008GL036952 by Cochrane France, Wiley Online Library on [02/06/2023]. See the Terms and Conditions (https://onlinelibrary.wiley.com/terms-and-conditions) on Wiley Online Library for rules of use; OA articles are governed by the applicable Creative Commons License

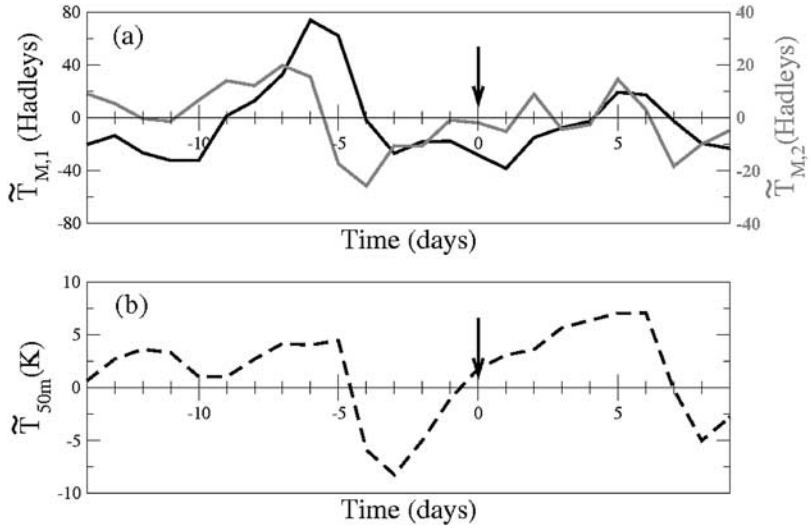


**Figure 3.** (a) $\widetilde{T}_{M,1}$ and $\widetilde{T}_{M,2}$ and (b) the average of $\widetilde{T}_{50m}$ over the sector [112.5°E; 117.5°E] × [25°N; 30°N]. The time axes for Figures 3a and 3b are in days relative to 14 November 1990 (black arrow).

[25] Figure 4a shows the composite of $\widetilde{R}_l$ averaged over the ESCS keyed on minus the IS $\widetilde{T}_{M,2}$ and on the IS $\widetilde{T}_{M,1}$. This composite shows that the OLR over the ESCS reaches a very significant minimum 2 to 4 days after a minimum in the intraseasonal $\widetilde{T}_{M,2}$. This positive 2–4 day lag is in agreement with the negative 2-day lag observed between $\widetilde{I}_C$ and $\widetilde{T}_{M,2}$ in Figure 1b. Figure 4a also shows that the OLR over the ESCS reaches a significant minimum 4 to 8 days after a maximum in the intraseasonal $\widetilde{T}_{M,1}$, which is coherent with the negative 5-day lag observed between $\widetilde{I}_C$ and $\widetilde{T}_{M,1}$ in Figure 1b.

[26] Figure 4b shows all the regions over which the composite of $\widetilde{R}_l$ keyed on the IS $\widetilde{T}_{M,1}$ has a significant negative peak (at the 99% significance level) between D+2 and D+10. This includes the SCS (not only the ESCS), but also the Bay of Bengal, northeastern India, most of the Mainland Southeast Asia, the Philippines, and Indonesia. The lag ranges between D+2 and D+8 depending on the regions, with a typical value of D+4 over the Bay of Bengal and Indonesia, D+6 over the ESCS and D+8 over the Philippines.

## 6. Conclusion

[27] The analyses presented in this paper reveal that the winter monsoon convective events over the ESCS are often preceded by large signals in both components of the EMT due to the Tibetan Plateau. These signals in the two components of the EMT are in lead-lag quadrature, and are associated with high surface pressure anomalies traveling from southern Siberia to the SCS within a week. The surface pressure and surface temperature patterns responsible for these relations

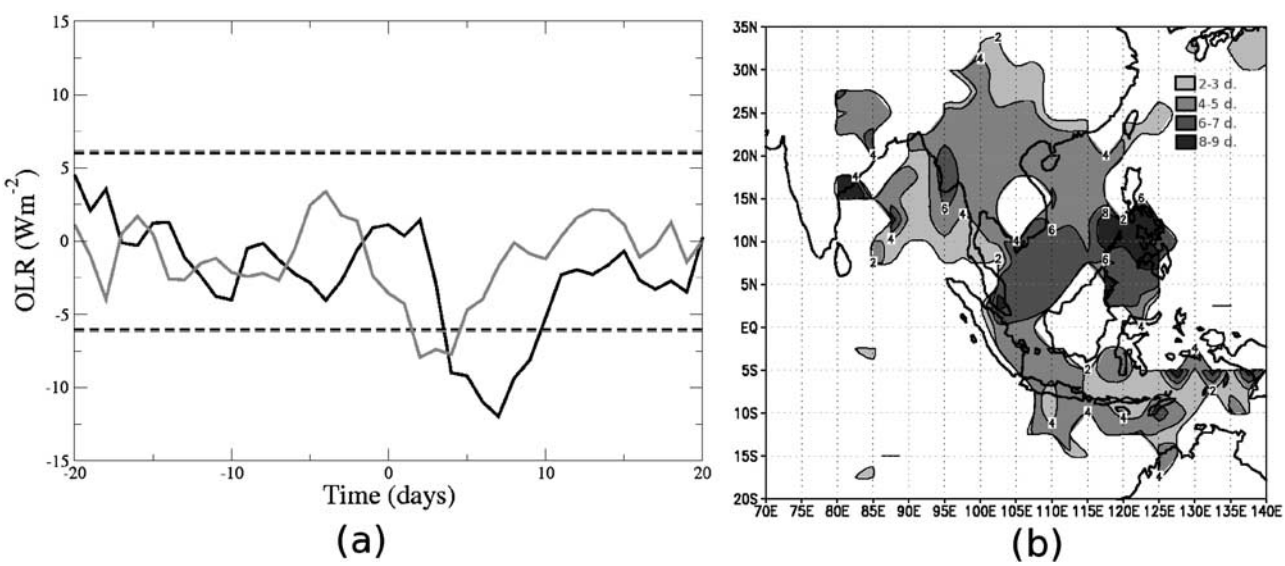


**Figure 4.** Composite series of the ESCS average OLR keyed on the IS $\widetilde{T}_{M,1}$ (black, solid) and on minus the IS $\widetilde{T}_{M,2}$ (gray, solid) and corresponding 99% significance levels (dotted). (b) Zones over which the OLR composite keyed on the IS $\widetilde{T}_{M,1}$ has a significant minimum at the 99% level between D+2 and D+9, and lag at which this minimum is reached (gray levels, in days after the peak of $\widetilde{T}_{M,1}$, see legend-box).



19448007, 2009, 6, Downloaded from https://agupubs.onlinelibrary.wiley.com/doi/10.1029/2008GL036952 by Cochrane France, Wiley Online Library on [02/06/2023]. See the Terms and Conditions (https://onlinelibrary.wiley.com/terms-and-conditions) on Wiley Online Library for rules of use; OA articles are governed by the applicable Creative Commons License

between the EMTs and the ESCS convection resemble the corresponding signals produced by the East Asian cold surges.

[28] To corroborate that the cold surges are in fact the vectors of these dynamical relations between the Tibetan plateau and the ESCS convection and to show that these relations are significant for the real weather, we have also analyzed one particular event characterized by very strong convection over the ESCS. This convective event is preceded by strong signals on the EMT components, and by a strong cold surge over southeast China.

[29] We have also found that the dynamical influence of the Tibetan Plateau on tropical convection is not limited to the ESCS: other regions such as the Bay of Bengal, Indonesia, and the north of the SCS have convection peaks in the days following the EMT events at the Tibetan Plateau.

[30] Our results suggest that the EMT affects the onset and the break of the winter monsoon active phases. They have some predictive interest in the sense that the signals on the torques precede by a few days and more these on the convection. From a more theoretical point of view, our results are related to the fact that the orography triggers lee anticyclones. As there is a large body of theoretical literature in mountain meteorology related to the development of lee cyclones [see, e. g., *Smith*, 1979], we will need to check if these theories can be adapted to our cases in order to understand our statistical results from a theoretical point of view.

[31] **Acknowledgments.** The NCEP Reanalysis data and Interpolated OLR data were kindly provided by the NOAA/OAR/ESRL PSD, Boulder, Colorado, USA, from their Web site at http://www.cdc.noaa.gov/.

## References

Blackmon, M. L. (1976), A climatological study of the 500 mb geopotential height of the Northern Hemisphere, *J. Atmos. Sci.*, *33*, 1607–1623.

Chang, C.-P., and K. M. Lau (1980), Northeasterly cold surges and near-equatorial disturbances over the winter MONEX area during December 1974. Part II: Planetary-scale aspects, *Mon. Weather Rev.*, *107*, 812–829.

Chang, C.-P., J. E. Erickson, and K. M. Lau (1979), Northeasterly cold surges and near-equatorial disturbances over the winter MONEX area during December 1974. Part I: Synoptic aspects, *Mon. Weather Rev.*, *107*, 812–829.

Chang, C.-P., Z. Wang, J. Ju, and T. Li (2004), On the relationship between western maritime continent monsoon rainfall and ENSO during northern winter, *J. Clim.*, *17*, 665–672.

Chang, C.-P., P. A. Harr, and H.-J. Chen (2005), Synoptic disturbances over the equatorial South China Sea and western Maritime Continent during boreal winter, *Mon. Weather Rev.*, *133*, 489–503.

Davies, H. C., and P. D. Phillips (1985), Mountain drag along the Gotthard section during ALPEX, *J. Atmos. Sci.*, *42*, 2093–2109.

Duchon, C. E. (1979), Lanczos filtering in one and two dimensions, *J. Appl. Meteorol.*, *18*, 1016–1022.

Egger, J., and K.-P. Hoinka (2000), Mountain torques and the equatorial components of global angular momentum, *J. Atmos. Sci.*, *57*, 2319–2331.

Egger, J., and K.-P. Hoinka (2008), Mountain torque events at the Tibetan Plateau, *Mon. Weather Rev.*, *136*, 389–404.

Feldstein, S. B. (2006), Dynamical processes of equatorial atmospheric angular momentum, *J. Atmos. Sci*, *63*, 565–581.

Fu, R., A. D. D. Genio, and W. B. Rossow (1990), Behavior of deep convective clouds in the tropical Pacific deduced from ISCCP radiances, *J. Clim.*, *3*, 1129–1152.

Garreaud, R. D. (2001), Subtropical cold surges: Regional aspects and global distribution, *Int. J. Climatol.*, *21*, 1181–1197.

Houze, R. A., S. G. Geotis, F. D. Marks, and A. K. West (1981), Winter monsoon convection in the vicinity of North Borneo. Part I: Structure and time variation of the clouds and precipitation, *Mon. Weather Rev.*, *109*, 1595–1614.

Hsu, H.-H., and J. M. Wallace (1985), Vertical structure of wintertime teleconnection patterns, *J. Atmos. Sci.*, *42*, 1693–1710.

Ichikawa, H., and T. Yasunari (2006), Time-space characteristics of diurnal rainfall over Borneo and surrounding oceans as observed by TRMM-PR, *J. Clim.*, *19*, 1238–1260.

Johnson, R., and D. L. Priegnitz (1986), Modification of the boundary layer over the South China Sea during a winter MONEX cold surge event, *Mon. Weather Rev.*, *114*, 2004–2015.

Kalnay, E., et al. (1996), The NCEP/NCAR 40-year reanalysis project, *Bull. Am. Meteorol. Soc.*, *77*, 437–471.

Liebmann, B., and C. Smith (1996), Description of a complete (interpolated) outgoing longwave radiation dataset, *Bull. Am. Meteorol. Soc.*, *77*, 1275–1277.

Lott, F. (1999), Alleviation of stationary biases through a mountain drag parameterization scheme and a simple representation of mountain lift forces, *Mon. Weather Rev.*, *127*, 788–801.

Lott, F., A. W. Robertson, and M. Ghil (2004), Mountain torques and Northern Hemisphere low-frequency variability. Part I: Hemispheric aspects, *J. Atmos. Sci.*, *61*, 1259–1271.

Murakami, T. (1980), Temporal variations of satellite-observed outgoing longwave radiation over the winter monsoon region. Part II: Short period (4–6 day) oscillations, *Mon. Weather Rev.*, *108*, 427–444.

Murakami, T. (1981), Orographic influence of the Tibetan Plateau on the Asiatic winter monsoon circulation, Part III. Short-period oscillations, *J. Meteorol. Soc. Jpn.*, *59*, 173–200.

Murakami, T., and H. Nakamura (1983), Orographic effects on cold surges and lee-cyclogenesis as revealed by a numerical experiment, Part II: Transient aspects, *J. Meteorol. Soc. Jpn.*, *61*, 547–567.

Nakamura, H., and T. Murakami (1983), Orographic effects on cold surges and lee-cyclogenesis as revealed by a numerical experiment, Part I: Time-mean aspects, *J. Meteorol. Soc. Jpn.*, *61*, 524–546.

Slingo, J. M. (1998), Extratropical forcing of tropical convection in a northern winter simulationn with the UGAMP GCM, *Q. J. R. Meteorol. Soc.*, *124*, 27–51.

Smith, R. B. (1979), Some aspects of the quasi-geostrophic flow over mountains, *J. Atmos. Sci.*, *36*, 2385–2392.

Sumi, A. (1983), A study on cold surges around the Tibetan Plateau by using numerical models, *J. Meteorol. Soc. Jpn.*, *63*, 377–396.

Zhang, Y., K. R. Sperber, and J. S. Boyle (1997), Climatology and interannual variation of the East Asian winter monsoon: Results from the 1979–95 NCEP/NCAR reanalysis, *Mon. Weather Rev.*, *125*, 2605–2619.

F. Lott and S. Mailler, LMD-ENS, 24 rue Lhomond, F-75231 Paris CEDEX 05, France. (flott@lmd.ens.fr)



19448007, 2009, 6, Downloaded from https://agupubs.onlinelibrary.wiley.com/doi/10.1029/2008GL036952 by Cochrane France, Wiley Online Library on [02/06/2023]. See the Terms and Conditions (https://onlinelibrary.wiley.com/terms-and-conditions) on Wiley Online Library for rules of use; OA articles are governed by the applicable Creative Commons License